# Built-in electric field assisted spin injection in Cr and Mn δ-layer doped AlN/GaN(0001) heterostructures from first principles

X. Y. Cui,[1] J. E. Medvedeva,[2] B. Delley,[3] A. J. Freeman,[4] and C. Stampfl[1]
[1]*School of Physics, The University of Sydney, Sydney 2006, New South Wales, Australia*
[2]*Department of Physics, Missouri University of Science and Technology, Rolla, Missouri 65409, USA*
[3]*Paul Scherrer Institut, WHGA/123, CH-5232 Villigen PSI, Switzerland*
[4]*Department of Physics and Astronomy, Northwestern University, Evanston, Illinois 60208-3112, USA*
(Received 16 October 2008; published 24 December 2008)

Highly spin-polarized diluted ferromagnetic semiconductors are expected to be widely used as ideal spin injectors. Here, extensive first-principles density-functional theory calculations have been performed to investigate the feasibility of using Cr- and Mn-doped wurtzite polar AlN/GaN(0001) heterostructures, with the aim to realize the appealing half-metallic character and, hence, efficient electrical spin injection. To overcome the formation of detrimental embedded clusters, we propose digital δ-layer doping perpendicular to the growth direction so as to realize enhanced performance at room temperature. The formation energy, electronic and magnetic properties, and the degree of spin polarization for both neutral and charged valence states for various concentrations are studied. Under both metal-rich (Al- or Ga-rich) and N-rich conditions, Cr and Mn dopants prefer to segregate into the GaN region and reside close to the interface, where dopant incorporation occurs more readily under N-rich conditions. The doped Cr and Mn atoms introduce 3*d* states in the band gap of the host semiconductor heterostructure. The spin injection channels are constructed via the hybridization between dopant 3*d* and surrounding host atoms, up to a few monolayers around the interface, where the spin-polarized $t_2$ electrons are injected into AlN without the conductivity mismatch problem. Significantly, for the energetically favorable configurations, the built-in electric field in the AlN/GaN(0001) heterointerface serves as a driving force for efficient spin injection through the interface and spin transport in the AlN region. Also importantly, the electronic properties of the heterostructures (half metallic, semiconducting, or metallic) are found to depend sensitively upon the doping concentration and valence charge states. In general, charged valence states can destroy the ferromagnetic half metallicity for both systems, particularly in *n*-type materials. These results will be useful with regard to the practical fabrication of desirable heterostructures for optoelectronic and semiconductor spintronic devices.

DOI: 10.1103/PhysRevB.78.245317 PACS number(s): 71.23.−k, 71.55.Eq, 75.50.−y, 85.75.−d

## I. INTRODUCTION

Recently, there has been a rapidly growing interest in the field of semiconductor spintronics, which aims to add spin-dependent functionality and enhanced performance to the existing principles of device operation. One of the crucial prerequisites, and still a challenge, for successful implementation of this concept is the ability to create a desired spin orientation of carriers and to transport them in a semiconductor to an active region of a device with minimum loss of spin polarization.[1–4] Traditionally, spin-polarized electrons have been created in semiconductors simply by illuminating the materials with circularly polarized light so that spin-polarized electrons with a preferred spin direction are excited (following the optical selection rules), enabling the generation of a spin-polarized current.[5] For practical spintronic device applications, however, electrical spin injection is required.

Electrical spin injection requires a contact material as the spin source (or spin aligner) and a corresponding interface that facilitates the transport of spin-polarized carriers into the semiconductor. The search for efficient spin injection contact materials falls broadly into two categories. One natural approach is to use ferromagnetic (FM) metal electrodes, such as Fe, which have a high Curie temperature ($T_C$) and low saturation field. The other approach is to use diluted magnetic semiconductors (DMSs).

For the first approach, initial attempts using diffusive Ohmic contacts harvested only poor efficiency—with spin polarization in the semiconductor typically much lower than 1%. Schmidt *et al.*[6] first rationalized that such difficulties were due to the "conductivity mismatch" between the metallic Ohmic contact and the semiconductor. They also argued that efficient spin injection can only be expected from highly spin-polarized metals, whereby traditional ferromagnetic metals typically do not meet this criterion. Shortly after, it was proposed that this intrinsic mismatch problem could be circumvented by insertion of a tunnel barrier between the metal and semiconductor.[7–9] This novel concept has paved the way for the subsequent success of significantly enhanced spin injection efficiency as demonstrated by several groups using a range of tunnel contacts, such as amorphous aluminum oxide and ordered MgO (for reviews, see Refs. 3 and 10). Typically, polarization values as large as 30–50 % were demonstrated at low temperature, while the polarization obtained at room temperature was much smaller. Furthermore, in order to drive enough current through the barrier, a considerable bias voltage must be applied across the junction, which could be a problem for spin detection.[11]

Within this framework, a unique class of materials, known as half-metallic ferromagnets, is particularly attractive. Half-metallic ferromagnets show a spin band completely empty at the Fermi level, which results in the appealing property of

 ©2008 The American Physical Society

conduction electrons being 100% spin polarized.[12] Some ferromagnetic transition-metal (TM) pnictides, such as CrAs (Ref. 13) and (half) Heusler alloys, such as NiMnSb, $Co_2MnGe$, and $Co_2CrAl$, whose bulk systems are predicted from first principles to be half metallic,[14,15] are under extensive investigation.[16] Studies show, however, that structural distortion and defects such as antisites and surfaces will typically destroy half metallicity (HM) and consequently degrade their performance.[13,17–19] Recently, it was theoretically predicted that for the $Co_2MnSi$/GaAs(001) heterostructure, only certain interface morphologies can conserve the half-metallic character.[20]

The other approach for spin injection involves DMSs as spin aligners. In principle, this has been expected to be the "ideal" choice for efficient electrical spin injectors and for semiconductor spintronic devices due to a number of superior properties.[4,10] First, DMSs have a conductivity comparable to that of most standard semiconductors so the mismatch problem is intrinsically eliminated.[21] Second, under certain conditions, DMSs normally have a spin polarization much higher than that found in metallic ferromagnets. Indeed, theoretical studies on DMSs often predict HM. Thus, it is expected that highly efficient spin injection and large magnetoresistance can be obtained when they are used as spin aligners and spin analyzers. Third, since DMSs can be grown epitaxially on device substrate semiconductors, they can be readily integrated with existing semiconductor technology. Fourth, from the device point of view, a purely semiconductor-based spintronics is more readily incorporated for signal processing and digital logic operations.[4]

The approach of spin injection from transition-metal-doped DMS was first suggested by Egues[22] through a theoretical consideration in a band-gap-matched (Zn, Mn)Se/ZnSe heterostructure. Subsequently, it was experimentally demonstrated by using either paramagnetic II-VI compounds such as BeMnZnSe (Ref. 23) and Mn:CdTe,[24] or ferromagnetic III-V compounds such as GaMnAs.[25] In the former II-VI-based DMS with a large ***g*** factor,[23] spin injection is facilitated in a band-gap-matched semiconductor structure containing a strong paramagnetic spin aligner. The spin polarization of the electron-doped system introduced above is nearly 100%. A drawback is that it is generally difficult to control conduction by doping in II-VI semiconductors. Moreover, due to the nature of the paramagnetic property, such devices need to be operated at very high magnetic fields and at very low temperatures to preserve the purity of the quantum states. An obvious remedy for this problem is the use of ferromagnetic semiconductors, for example, III-V-type DMS such as Mn:GaAs, as a spin aligner.[25] The *p*-type ferromagnetic semiconductor Mn:GaAs has been a paradigmatic DMS studied so far for spin injection. However, it suffers from the limitation of its $T_C$ to low temperature ($\sim$170 K), which precludes its practical use in room-temperature devices.

Quite recently, many groups have focused on transition-metal-doped (particularly Mn- and Cr-doped) wide-band-gap GaN- and AlN-based DMSs. One of the reasons is the prediction of room-temperature ferromagnetism by Dietl *et al.*[26] on the basis of a mean-field Zener model. Subsequently, various groups have experimentally reported ferromagnetism with $T_C$ well above room temperature up to 900 K for Cr:GaN (Refs. 27–30) and Mn:GaN (Refs. 31 and 32) although the origin of the ferromagnetism is still a subject of debate, particularly for Mn-doped GaN.[33,34] Furthermore, for spintronic devices, it is critical that after injection of spin-polarized electrons into a semiconductor, the spin dephasing during transport must be negligible. The III nitrides are more robust to high defect densities than GaAs (Ref. 35) and the spin lifetime in GaN is predicted to be 3 orders of magnitude larger than that in GaAs due to the larger conduction-band density of states (DOS) and smaller spin-orbit coupling.[36] In addition, another attractive property is that the transition-metal-doped (such as Mn- and Cr-doped) III-nitride DMSs have been predicted to be half metallic[37] under certain conditions, which we will discuss in detail below. Recently, we predicted that in the Cr:AlN/GaN(0001) heterostructures, Cr atoms segregate into the GaN region, and more importantly, the interfaces can retain the desirable half-metallic behavior of the separate Cr:AlN and Cr:GaN systems. Thus, we proposed the possibility of achieving efficient spin injection from a ferromagnetic Cr:GaN electrode through an AlN tunnel barrier.[38] Similar novel properties were also predicted for Mn:GaN/AlN(0001) systems.[39]

These desirable properties indicate that TM-doped III-nitride DMSs are excellent candidates for high-efficiency magnetoelectronic devices. However, despite some encouraging aspects, so far the experiments have yielded unsatisfying results in terms of spin injection efficiency.[40,41] Kim *et al.*[40] reported spin-dependent transport in fully epitaxial GaCrN/AlN/GaCrN trilayer heterostructures with different Cr concentrations grown by molecular-beam epitaxy (MBE). Well-defined hysteresis loops were observed in the magnetization versus magnetic field curves even at room temperature. However, the tunnel magnetoresistance (TMR) ratio is only 0.1%, indicating a very low spin polarization at the GaCrN/AlN interfaces. Ham *et al.*[41] demonstrated electrical spin injection from room-temperature ferromagnetic (Ga, Mn)N in nitride-based spin-polarized light-emitting diodes. They found that the anomalous Hall resistance is proportional to the out-of-plane magnetization. These results support the notion that (Ga, Mn)N is an appropriate material for a spin injection source in room-temperature-operating semiconductor spintronic devices. Again, however, a very low spin injection efficiency was obtained—the electroluminescence polarization saturates around 8 T and reaches maximum values of approximately 1.3% and 0.8% at 150 and 300 K, respectively.

Clearly, an improved understanding of the dependence of the materials used on the growth and fabrication conditions, and the nature of the interfaces will provide essential input for successful spin injection and optimization of device design and performance. Thus understanding of the large discrepancy between theoretical expectations and experimental observations has been a major motivation of the present study. Unlike the metal electrodes for which the magnetic and electronic properties have been well understood, the DMS itself is still a subject under intense research. In particular, regarding the predicted HM in III-nitride-based DMS, experiments showed that Cr:GaN (Refs. 42 and 43) and Mn:GaN (Refs. 44 and 45) are in fact semiconducting or

highly insulating. Moreover, the observed magnetic moments are much smaller than expected. We argue that one of the key issues concerns the spatial distribution of the doped ions: while most first-principles calculations assume a homogeneous distribution, experiments show that dopants prefer to form clusters—incorporated with the host matrix but along the epitaxial growth direction.[46] Recently, we showed that such energetically favorable embedded clusters can greatly affect the electronic and magnetic properties such as the magnetic interaction and moments. Moreover, the electrical conductivity competition between half-metallic, semiconducting, or metallic character sensitively depends on concentration and dopant distribution[47,48] and charged states, particularly for Mn-doped III nitride under $n$-type conditions.[34]

Such clustering is detrimental for performance and could be hard to avoid under nonequilibrium conventional epitaxial growth conditions due to the attractive interaction among dopants. In view of the fact that such clusters prefer to form along the growth direction during the layer-by-layer epitaxial growth process, to eliminate the formation of these embedded clusters, we propose a growth method to confine the dopants in the $x$-$y$ plane, namely, the $\delta$-layer epitaxial doping of Mn or Cr perpendicular to the growth direction. Technically, it has been well established that digital $\delta$-function-like doping profiles can be obtained in III-V semiconductors by growth-interrupted impurity deposition during molecular-beam epitaxy,[49] and it is expected to be an effective approach to realize high $T_C$ and to overcome phase precipitates.[50,51]

Another motivation of this study is to investigate the effects of the built-in electric field on spin injection in wurtzite AlN/GaN(0001) heterostructures. Recently, Litvinov[52] derived a novel concept that spin injection can be considerably enhanced up to several orders of magnitude by the built-in electric field in a piezoelectric AlGaN/GaN double-barrier structure. Thus, the intrinsic electric field can be engineered for manipulation of the spin injection efficiency in prospective spintronic devices. It is well known that wurtzite AlN and GaN have large piezoelectric constants,[53] and huge built-in electric fields have been theoretically predicted[54] and experimentally demonstrated[55] in the forms of superlattices and multilayers. Thus, the Cr- and Mn-doped polar AlN/GaN(0001) heterostructures serve as a prototype system to investigate in detail such an effect on spin injection.

Compared with using metal ferromagnets as spin injectors, DMS-based spin injection systems are at a much earlier stage of development largely because of the poor understanding of the DMS itself. In this paper, we investigate the structural, energetic, electronic, and magnetic properties of pure and $\delta$-layer Cr- and Mn-doped polar AlN/GaN(0001) heterostructures, for which both neutral and charged states are considered. We demonstrate the DMS-based spin injection at the atomic level. We address how the dopant concentration and charged states may affect the conductivity and spin injection efficiency, which is largely unexplored to date. Indeed, the conducting properties of the heterostructures (half metallic, semiconducting, or metallic) are found to depend sensitively upon the doping concentration and valence charge states, similar to the separate Cr- and Mn-doped GaN and AlN components.[34,47,48] Charged valence states can further destroy the ferromagnetic half metallicity for both Cr- and Mn-doped AlN/GaN interface systems, particularly in $n$-type materials. Furthermore, we study the role of the built-in electric field in pure and doped heterostructures and its correlation with spin injection. Indeed, we find that it can be employed as the driving force and, thus, can enhance the spin injection and the subsequent spin transport in AlN for the energetically most favorable doped configurations. These results should be useful for the practical fabrication of desirable heterostructures and could be also applied for other DMS systems.

## II. COMPUTATIONAL DETAILS

We perform extensive density-functional theory (DFT) calculations using both the local-density approximation (LDA) (Ref. 56) and the generalized gradient approximation (GGA) (Ref. 57) for the exchange-correlation functional as implemented in the DMol$^3$ code.[58] DMol$^3$ employs fast converging three-dimensional numerical integrations to calculate the matrix elements occurring in the Ritz variational method. The wave functions are expanded in terms of a double-numerical quality localized basis set with a real-space cutoff of 9 bohr. Polarization functions and scalar-relativistic corrections are incorporated explicitly. Density-functional semilocal pseudopotentials[59] are employed. In this scheme, all electrons for N and Al are included, while for Ga, Cr, and Mn the $3d^{10}4s^2 4p^1$, $3s^2 3p^6 3d^5 4s^1$, and $3s^2 3p^6 3d^5 4s^2$ electrons are treated as valence electrons, respectively. For some key properties, we also confirmed our results by performing all-electron calculations. Except where specified, full relaxation, including the atomic positions and lattice constants, is performed in all calculations. For the pure and doped interface structures, we deliberately enforce no symmetry constraints. We employ variously sized supercells ranging from 12 to 192 atoms to address the effect of concentration for Cr-doped AlN, GaN, and their interfaces. The Brillouin-zone integrations are performed using an $8 \times 8 \times 4$ Monkhorst-Pack grid for the 32-atom ($2a \times 2a \times 2c$, where $a$ and $c$ are the lattice constants of the unit cells) doped GaN or AlN supercells, yielding 35 **k** points in the irreducible part of the Brillouin zone. For the other supercells, the grids have been obtained such that the same or similar sampling of reciprocal space is obtained. Convergence parameters, 5 meV for the total energy, $8 \times 10^{-2}$ eV/Å for the force, and $1 \times 10^{-2}$ Å for the atomic displacements are used.

It has been established, from both experiments and calculations, that the doped Cr and Mn atoms prefer to substitute cations in both GaN and AlN (Refs. 34, 48, and 60); hence in this study, only substitutional (on Ga or Al) sites are considered. We calculate the formation energy for the neutral and charged states to determine the relative stability of the different configurations,[61] for which the formation energy for a charged state $q$ for a given configuration is calculated as

$$E_D^f = E_D - E_{\mathrm{ref}} + \sum n_\alpha \mu_\alpha + q(E_F + E_V + \Delta V), \qquad (1)$$

where $E_D$ is the total energy of the doped systems, [i.e., Cr-, Mn-doped GaN, AlN, or AlN/GaN(0001)] and $E_{\mathrm{ref}}$ is the corresponding pure reference structure as calculated for the same size supercell. $n_\alpha$ is the number of atoms removed (+)

or added (−) to the host; $\mu_\alpha$ is the chemical potential of Cr (or Mn) and Al (or Ga) atoms; $E_F$ is the variable Fermi level, referenced to the valence-band maximum in bulk GaN (or AlN); and $E_V$ is the bulk valence-band maximum of the reference supercell. The correction term, $\Delta V$, is used to align the reference electrostatic potential between the supercell containing the charged defect and the bulk supercell.

Now, the chemical potentials depend on the experimental conditions under which the material is grown. In order to determine these quantities, we invoke the relationship $\mu_{Ga}+\mu_N=\mu_{GaN}$ and $\mu_{Al}+\mu_N=\mu_{AlN}$, namely, assuming the atom species are in thermal equilibrium with GaN or AlN. When imposing certain growth conditions, namely, nitrogen-rich ($\mu_N=1/2\mu_{N_2}$) or metal-rich [gallium-rich ($\mu_{Ga}=\mu_{Ga(bulk)}$)] or aluminum-rich ($\mu_{Al}=\mu_{Al(bulk)}$) conditions, the chemical potential for the other species can be determined as follows: since we are not aware of crystallographic data or formation energy data for the Cr-Al and Cr-Ga systems, the chemical potential for Cr atom is assumed to be determined by equilibrium with bulk $Cr_2N$, which is the most stable chromium nitride. Thus, under nitrogen-rich conditions, $\mu_{Cr}=1/2[E_{Cr_2N}-1/2E_{N_2}]$, $\mu_{Ga}=E_{GaN(bulk)}-1/2E_{N_2}$, or $\mu_{Al}=E_{AlN(bulk)}-1/2E_{N_2}$; under gallium-rich conditions, $\mu_{Cr}=1/2[E_{Cr_2N(bulk)}-(E_{GaN(bulk)}-E_{Ga(bulk)})]$ and $\mu_N=1/2[E_{GaN(bulk)}-E_{Ga(bulk)}]$; or under aluminum-rich conditions, $\mu_{Cr}=1/2[E_{Cr_2N(bulk)}-(E_{AlN(bulk)}-E_{Al(bulk)})]$ and $\mu_N=1/2[E_{AlN(bulk)}-E_{Al(bulk)}]$. For Mn-doped GaN, AlN, and their heterostructures, the chemical potential for Mn atom is evaluated by assuming thermal equilibrium with rocksalt MnN-type and CuAu-type GaMn (or AlMn) under N-rich and Ga-rich conditions, respectively. Thus, under N-rich conditions, $\mu_{Mn}=E_{MnN(bulk)}-1/2E_{N_2}$, and under Ga-rich (or Al-rich) conditions, $\mu_{Mn}=E_{GaMn(bulk)}-E_{Ga(bulk)}$ [or $\mu_{Mn}=E_{AlMn(bulk)}-E_{Al(bulk)}$]. Further computational details, including results for bulk Al, Ga, Cr, Mn, and the free nitrogen molecule, can be found in Refs. 34 and 48.

The key parameter determining and evaluating spin injection efficiency is the spin polarization $P$ at the Fermi level, defined as[19]

$$P=\frac{N^{\uparrow}(E_F)-N^{\downarrow}(E_F)}{N^{\uparrow}(E_F)+N^{\downarrow}(E_F)}, \tag{2}$$

where $N^{\uparrow}(E_F)$ and $N^{\downarrow}(E_F)$ donate the majority and minority-spin channel DOS at the Fermi level, respectively. Half-metallic magnets possess a 100% spin polarization at the Fermi energy while semiconducting states correspond to $P=0$. For metallic states, both majority and minority spins are expected to be injected, resulting in less than 100% efficiency. For half-metallic magnets, another important parameter affecting the spin injection efficiency is the absolute value of the DOS at the $E_F$.

## III. RESULTS AND DISCUSSION

### A. Undoped and doped AlN and GaN

We first study the parent compounds—bulk wurtzite AlN and GaN. The calculated equilibrium properties including lattice constants, bulk modulus, cohesive energy, formation enthalpy, and band-gap values using both the GGA and LDA are summarized in Table I and are compared with other first-principles studies and experiments.[62–64] Overall, as expected, the GGA gives larger lattice constants, smaller bulk moduli, smaller cohesive energy and formation enthalpy, and smaller band-gap values, as compared with the LDA results. Regarding energetics, the GGA gives considerably closer agreement with experiments than the LDA, which exhibits the well-known overbinding, as found in Refs. 63 and 64. Discrepancies of bulk moduli, energy values and band gaps between the LDA and GGA are primarily due to the larger lattice constant obtained using the GGA compared to the LDA, i.e., to deformation-potential effects, as pointed in Ref. 63. Such volume-dependent effects are particularly predominant for the band-gap values. The calculated GGA direct band gap is about 10% (0.46 eV) and 18% (0.56 eV) smaller than the LDA values for AlN and GaN, respectively.

Before assembling the Cr- and Mn-doped AlN/GaN(0001) interfaces, we calculated the formation enthalpy for Cr- and Mn-doped bulk GaN and AlN under metal-rich and N-rich conditions in 32-atom supercells. The calculated formation energies and magnetic moments are shown in Table II. It can be seen that under both N-rich and metal-rich growth conditions, both LDA and GGA predict that the formation energies of AlN-based systems are considerably larger (about 1.4–1.6 eV) than GaN-based ones, showing it is easier to introduce Cr and Mn into GaN than into AlN. This can be understood, to a first approximation, by considering (i) the larger lattice constants, thus, larger space at the cation site in GaN than in AlN; (ii) ionic size matching—i.e., the radii of $Cr^{3+}$ (0.61 Å) and $Mn^{3+}$ (0.58 Å) are larger, but much closer to $Ga^{3+}$ (0.47 Å), than to $Al^{3+}$ (0.39 Å) in a tetrahedral environment.[65] The LDA predicts higher formation energies than the GGA by about 0.5 eV. For all four systems, the formation energy under N-rich conditions is lower than under metal-rich conditions. Moreover, N-rich conditions will suppress the formation of interstitial configurations as reported in Refs. 34 and 48, suggesting that optimal growth conditions should be N rich. As for the magnetic moments, both the LDA and GGA predict that Cr-doped GaN and AlN systems have a total magnetic moment of $3\mu_B$ per cell, while Mn doped systems have a total value of $4\mu_B$ per cell. It is also found that the magnetic moments in Cr-doped systems are very localized on Cr atoms (very close to $3\mu_B$), while in Mn-doped systems, the moments are more spread out spatially.

### B. Pure AlN/GaN(0001) interfaces

We construct variously sized $(AlN)_n/(GaN)_n(0001)$ interfaces in this study, where $n$ represents the number of double nitride layers. In the $x$-$y$ plane, we use $(1\times1)$, $(1\times2)$, $(2\times2)$, and $(4\times4)$ supercells, and the $z$ direction is perpendicular to the interface plane. As an example, Fig. 1 shows the $(1\times2):(AlN)_5/(GaN)_5(0001)$ structure; for short, we label it as the "$(1\times2):5+5$" heterointerface. It contains two regions (AlN and GaN) and two different interfaces (type A and type B), where the type-I interface refers to AlN/GaN(0001) and the type-II interface to GaN/AlN(0001).

TABLE I. Lattice constants ($a$ and $c$), internal parameters $u$, bulk moduli $B$, cohesive energies $E_c$, formation enthalpies $\Delta H$, and band gaps $E_g^{\Gamma}$ of wurtzite AlN and GaN.

| Method | $a$ (Å) | $c$ (Å) | $u$ | $B$ (Mbar) | $E_c$ (eV) | $\Delta H$ (eV) | $E_g^{\Gamma}$ (eV) |
|---|---|---|---|---|---|---|---|
| | | | | AlN | | | |
| Present GGA | 3.137 | 5.002 | 0.3831 | 1.96 | 12.313 | −3.013 | 4.27 |
| Present LDA | 3.006 | 4.935 | 0.3832 | 2.32 | 13.596 | −3.514 | 4.73 |
| GGA[a] | 3.110 | 4.994 | 0.3819 | | 12.071 | −3.142 | |
| LDA[a] | 3.070 | 4.910 | 0.3821 | | 13.536 | −3.642 | |
| GGA[b] | 3.113 | 5.041 | 0.3798 | 1.92 | 11.403 | | 4.245 |
| LDA[b] | 3.057 | 4.943 | 0.3802 | 2.09 | 13.286 | | 4.74 |
| LDA[c] | 3.085 | 4.993 | | | | | 4.34 |
| sX-LDA[c] | | | | | | | 6.05 |
| Expt.[a,b,d] | 3.111 | 4.978 | 0.385 | 1.85–2.12 | 11.669 | −3.13 | 6.28 |
| | | | | GaN | | | |
| Present GGA | 3.189 | 5.182 | 0.3765 | 1.84 | 10.125 | −1.040 | 2.58 |
| Present LDA | 3.128 | 5.079 | 0.3761 | 2.09 | 11.386 | −1.452 | 3.14 |
| GGA[a] | 3.199 | 5.226 | 0.3772 | | 9.265 | −1.118 | |
| LDA[a] | 3.131 | 5.104 | 0.3768 | | 10.999 | −1.685 | |
| GGA[b] | 3.245 | 5.296 | 0.3762 | 1.72 | 8.265 | | 1.45 |
| LDA[b] | 3.193 | 5.218 | 0.376 | | 10.187 | | 1.76 |
| LDA[c] | 3.142 | 5.194 | | | | | 2.00 |
| sX-LDA[c] | | | | | | | 3.35 |
| Expt.[a,b,d] | 3.180 | 5.166 | 0.375 | 1.88–2.45 | 9.058 | −1.08 | 3.41 |

[a]Reference 62.
[b]Reference 63.
[c]Reference 38.
[d]Reference 64.

The in-plane $x$-$y$ lattice parameters $a$ of the pure AlN and GaN differ by 1.38% (GGA) and 0.39% (LDA), compared with the experimental value of 2.20%, with the one of GaN being larger. Epitaxial growth of AlN/GaN(0001) interfaces will introduce a built-in biaxial strain due to this lattice mismatch. The shear components will lower the symmetry of the system and split the highly degenerate electronic levels, which may cause considerable changes in the values of the band gap. Most of the strain can be released around the interface area through lattice distortion. We have examined the convergence of this effect by using $(1\times2)$:$(\mathrm{AlN})_n$/$(\mathrm{GaN})_n$(0001) supercells (using the GGA), where the double layer number $n$ varies from 1 to 7 (i.e., 4–28 atoms per supercell). Two criteria are considered to examine the convergence behavior; namely, (i) around the interface, the local properties, such as bond lengths (shown as B1, B2, and B3 in Fig. 1) and Mulliken atomic charge distributions (on Al1 and Ga1), should exhibit no appreciable change upon increasing the number of double layers $n$. (ii) Away from the interface,

TABLE II. Atomic magnetic moments (MMs) on dopants (Cr or Mn) and formation energy values under metal-rich, $E^f_{\mathrm{metal}}$, and N-rich, $E^f_{\mathrm{N}_2}$, conditions for Cr- and Mn-doped bulk AlN and GaN (calculated using 32-atom supercells).

| | GGA | | | LDA | | |
|---|---|---|---|---|---|---|
| System | $E^f_{\mathrm{metal}}$ (eV) | $E^f_{\mathrm{N}_2}$ (eV) | MM ($\mu_B$) | $E^f_{\mathrm{metal}}$ (eV) | $E^f_{\mathrm{N}_2}$ (eV) | MM ($\mu_B$) |
| Cr:AlN | 4.44 | 2.93 | 2.94 | 5.35 | 3.59 | 2.83 |
| Cr:GaN | 1.99 | 1.48 | 2.97 | 2.85 | 2.12 | 2.89 |
| Mn:AlN | 5.64 | 4.13 | 3.83 | 6.46 | 4.70 | 3.72 |
| Mn:GaN | 3.06 | 2.54 | 3.81 | 3.94 | 3.21 | 3.69 |

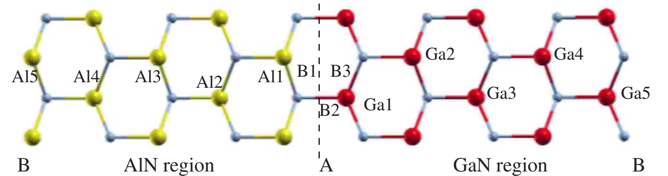


FIG. 1. (Color online) Geometry of the $(1\times2)$:$(\mathrm{AlN})_5$/$(\mathrm{GaN})_5$(0001) heterostructure. Substitutional sites considered for Cr (or Mn) atoms are labeled as "Al1," "Al2," etc. The center (middle dashed line) represents the type-A interface while the two edges correspond to the type-B interface. Small (green) spheres indicate N atoms and large spheres; light (yellow) and dark (red) spheres indicate Al and Ga atoms, respectively. The labels "B1," "B2," and "B3" indicate the bonds around the type-A interface.

TABLE III. Variation in the band gap, Mulliken charge, and bond length as a function of the layer thickness using $(1\times2):(\mathrm{AlN})_n/(\mathrm{GaN})_n(0001)$, as obtained from GGA.

| No. of layers $(n+n)$ | Band gap (eV) | Mulliken charge Al1 | Mulliken charge Ga1 | Bond length (Å) B1 | Bond length (Å) B2 | Bond length (Å) B3 |
|---|---|---|---|---|---|---|
| 1+1 | 3.36 | 2.002 | 0.046 | 1.911 | 1.908 | 1.936 |
| 2+2 | 3.29 | 1.722 | 0.340 | 1.910 | 1.954 | 1.933 |
| 3+3 | 3.16 | 1.735 | 0.332 | 1.910 | 1.963 | 1.931 |
| 4+4 | 3.03 | 1.732 | 0.329 | 1.909 | 1.954 | 1.933 |
| 5+5 | 2.91 | 1.728 | 0.330 | 1.909 | 1.954 | 1.933 |
| 6+6 | 2.77 | 1.727 | 0.330 | 1.909 | 1.954 | 1.933 |
| 7+7 | 2.59 | 1.727 | 0.330 | 1.909 | 1.954 | 1.933 |

such properties should be converged to those in bulk AlN and GaN. The corresponding bond lengths are B1 =1.904 Å and B2=1.920 Å in pure AlN and B2=1.952 Å and B3=1.945 Å in pure GaN. We find that these two criteria are satisfied with $n\geq4$ (see Table III). In this study, we employ $n=3$ and $n=5$ (i.e., 3+3 and 5+5 structures) to study the doped heterostructures. Table IV lists the fully relaxed lattice constants and band-gap values of the superlattices using both the GGA and LDA. It can be seen that for $n\geq4$ the in-plane lattice constants are almost unchanged, remaining 0.7% and 2.7% larger (0.69% and 0.61% smaller) than that of bulk AlN (GaN), as obtained using GGA and LDA, respectively.

We calculated the DOS and band structure. The band structure and total DOS using the GGA for pure GaN, AlN, and $(1\times1):(\mathrm{AlN})_n/(\mathrm{GaN})_n(0001)$ ($n=3$ and 5) heterostructures are displayed in Fig. 2. For both AlN and GaN, the displayed total DOS presents three regions: the lower part of the valence bands is dominated by N 2*s* (−18 to −15 eV) states, and the upper part (−8.5 to −2.5 eV for AlN, and −8.0 to −1.8 eV for GaN) is formed from N 2*p* hybridized with Al 3*p* and Al 3*s* states for AlN and GaN 3*p* and 3*s* for GaN, in which the Al 3*s* and Ga 3*s* contribute to lower valence bands. The lowest conduction band at the Γ point is predominantly of Al 3*s* (GaN 3*s*) character and located at 2.3 eV for AlN (1.5 eV for GaN). After forming superlattices, the position of these three regions is mainly unchanged. One can see

TABLE IV. Lattice constants *a* and *c* and band gaps $E_g^\Gamma$ for the $(1\times1):(\mathrm{AlN})_n/(\mathrm{GaN})_n(0001)$ ($n=3$ and 5) superlattices.

| Method | $a$ (Å) | $c$ (Å) | $E_g^\Gamma$ (eV) |
|---|---|---|---|
| | $(1\times1):(\mathrm{AlN})_3/(\mathrm{GaN})_3$ | | |
| GGA | 3.159 | 15.266 | 3.16 |
| LDA | 3.088 | 14.956 | 3.72 |
| | $(1\times1):(\mathrm{AlN})_5/(\mathrm{GaN})_5$ | | |
| GGA | 3.159 | 25.428 | 2.91 |
| LDA | 3.089 | 24.897 | 3.38 |

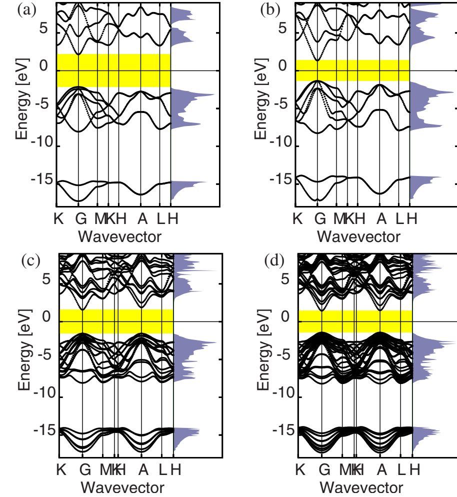


FIG. 2. (Color online) Band structure and total density of states of (a) bulk AlN, (b) bulk GaN, (c) $(1\times1):(\mathrm{AlN})_3/(\mathrm{GaN})_3(0001)$, and (d) $(1\times1):(\mathrm{AlN})_5/(\mathrm{GaN})_5(0001)$ superlattices.

clearly that the semiconducting behavior of AlN and GaN is retained in the AlN/GaN(0001) heterostructures, with the 5 +5 systems having a decreased direct band gap compared with the 3+3 counterpart. Interestingly, including full optimization of the lattice constants and relaxation of all the atoms, both GGA and LDA calculations predict that the band gap decreases monotonically with the number of layers in the superlattice. This rather astonishing behavior is due to the strong built-in electric field as reported in Ref. 66. Both wurtzite AlN and GaN possess a spontaneous polarization, and because of the strain at the interface, there is an additional piezoelectric contribution to the total polarization. The polarizations in both materials are different and lie perpendicular to the (0001) interface because of the symmetry cancellation in the *x*-*y* plane. Consequently, there is a polarization charge accumulation at the interface and a spontaneous built-in electric field throughout the heterostructure.

To further demonstrate this effect, we present the N-atom 1*s* core-level binding energies $E_b^{\mathrm{CL}}$ of each layer for the $(\mathrm{AlN})_5/(\mathrm{GaN})_5(0001)$ heterostructure, as shown in Fig. 3. It can be clearly seen that there is a different slope of the curves at the AlN (negative) and GaN (positive) regions,

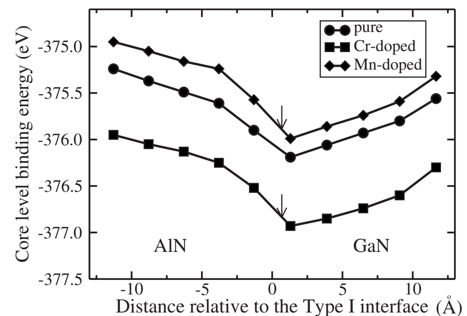


FIG. 3. Nitrogen 1*s* core-level binding energies in pure and Cr- and Mn-doped $(1\times2):(\mathrm{AlN})_5/(\mathrm{GaN})_5(0001)$ heterostructures in the neutral state using the GGA. The arrows indicate the energetically most favorable δ-layer doped positions.

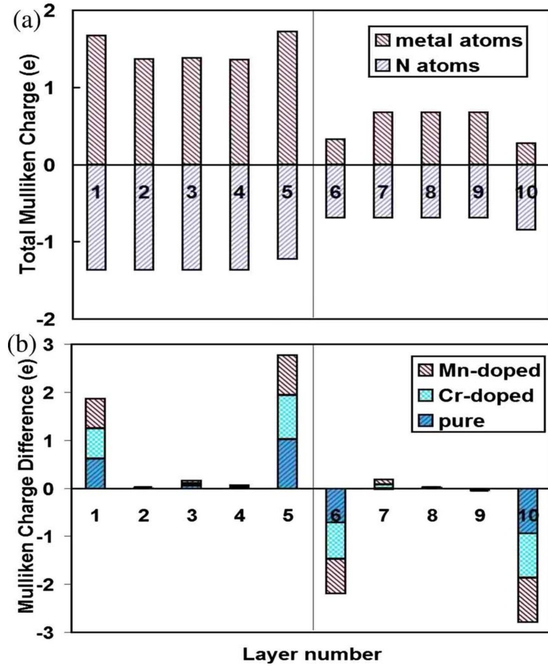


FIG. 4. (Color online) Demonstration of the charge accumulation and the built-in electric field in pure and Cr- and Mn-doped $(1\times2):(AlN)_5/(GaN)_5(0001)$ heterostructures using the GGA. (a) The total Mulliken charge of different double layers in the pure superlattice. (b) The Mulliken charge difference in pure and Cr- and Mn-doped heterostructures.

showing that the electric fields have opposite signs at the two sides of the interface.[67] Following the method outlined in Ref. 68, the slopes of the linear trends give a rough estimate of the absolute values of the electric fields ($|\mathbf{E}|=\Delta E_b^{CL}/\Delta z$), where $\Delta E_b^{CL}$ is the difference in $E_b^{CL}$ of the N atoms with a distance of $\Delta z$ along the (0001) direction. The calculated value is about $4\times10^8$ V/m in both the AlN and GaN sides of the heterostructure; this value is significantly larger than those calculated for the GaSb/InSb [111] ($3\times10^7$ V/m) and GaSb/InSb [111] ($1.2\times10^8$ V/m) heterostructures.[68] Around the interface region, the electric field is even stronger, with an estimated value of $1\times10^9$ V/m. Our predicted average intrinsic electric field strength in $(AlN)_5/(GaN)_5(0001)$ is $6.3\times10^8$ V/m, which compares reasonably well with experimental values of 5.04 and 6.07 $\times10^8$ V/m for 20-period $(AlN)_8/(GaN)_{10}$ and $(AlN)_8/(GaN)_6$ superlattices, respectively.[55]

Such a strong spontaneous electric field corresponds to a charge accumulation around the interfaces, which mainly arises from the spontaneous dielectric polarization of the hexagonal phase, and the strain-induced piezoelectric polarization.[69] To demonstrate this effect, we calculate the average (per N or per metal atom) Mulliken atomic charge and the Mulliken charge difference[70] (total charge minus the corresponding charge in bulk AlN and GaN) for each double layer in the $(1\times2):(AlN)_5/(GaN)_5(0001)$ interface (each double layer contains two N atoms and two Al or Ga atoms), as shown in Figs. 4(a) and 4(b). The different double layers along the growth direction are labeled from left to right in progressive order (from 1 to 10). The inhomogeneous charge distribution is clearly demonstrated. For the total Mulliken charge in Fig. 4(a), it can been seen that the Al atoms in the AlN region have more abundant (positive) Mulliken charge than the Ga atoms in the GaN region; this can be understood from the relative values of the atomic electronegativity (Al: 1.61; Ga: 1.81; and N: 3.04). In contrast to the case of bulk AlN and GaN, around the interfaces, the values of the sum of the Mulliken charge of metal (Al or Ga) and N atoms are nonzero—showing charge accumulation. Within the bulk region (layers 2–4 in AlN, and layers 7–9 in GaN), there are roughly constant charge populations at both N atoms and metal (Al or Ga) atoms, resulting in negligible net charge accumulation, as shown in Fig. 4(b). By contrast, around both interfaces (type A between layers 5 and 6 and type B between layers 10 and 1 in the neighboring supercell, with periodic boundary conditions), there is opposite large charge accumulation, forming large opposite interface dipoles at type-A and type-B interfaces, and resulting in the strong built-in electric field throughout the heterostructure. We have also checked the charge distribution using thicker superlattices, e.g., $(AlN)_7/(GaN)_7$ and $(AlN)_9/(GaN)_9(0001)$, and obtain the same conclusion. This shows that the charge accumulation acts like a microscopic capacitor effect on an atomic scale.[71]

### C. Cr- and Mn-doped AlN/GaN(0001) interfaces

#### *1. Neutral states*

While the presence of interfaces breaks the symmetry of pure AlN and GaN in the (0001) direction, doping of a Cr atom further decreases the symmetry in the *x-y* plane. In order to study the effect of dopant concentration, we systematically simulate the $(AlN)_n/(GaN)_n(0001)$ ordered interfaces with various in-plane sizes, namely, $(1\times1)$, $(1\times2)$, and $(2\times2)$ for both $n=3$ and 5, corresponding to dopant concentrations of 1, 1/2, and 1/4 monolayer (ML), respectively. For certain configurations, we also checked a $(4\times4)$ structure for $n=3$, which corresponds to a low concentration of 1/16 ML. To determine the energetically most favorable doping site, we considered substitution on the Ga or Al sites in each layer. For example, the doped sites considered in the $(1\times2):(AlN)_5/(GaN)_5(0001)$ heterostructure are shown in Fig. 1. As expected, based on the results for the bulk systems, under both metal-rich and N-rich growth conditions, the formation energy shows that both Cr and Mn atoms prefer to segregate into the GaN region. The calculated formation energies in the AlN region are about 1.5 eV higher than in the GaN region, similar to the case of the doped parent compounds. In the same component (either AlN or GaN) region, the formation energies are very competitive. For example, for the $(1\times2):(AlN)_5/(GaN)_5(0001)$ system, the relative energies between the five Al sites for Cr or Mn are within 15 meV, and for the five doped Ga sites they vary by less than 35 meV. Importantly, in the favorable GaN region, the site closest to the interface is always favored, regardless of the concentration, i.e., whether we consider one Cr (or Mn) in the $(1\times1)$, $(1\times2)$, or $(2\times2)$ supercells. The most favorable site is Ga1, which is closest to the type-A interface. The next most favorable is the Ga site closest to the type-B

TABLE V. MMs on the Cr atom, and the formation energies under metal-rich, $E^f_{\mathrm{metal}}$, and N-rich, $E^f_{\mathrm{N_2}}$, growth conditions, and the spin polarizations $P$ for the energetically most favorable Cr-layer doped $(1\times1)$, $(1\times2)$, and $(2\times2):(\mathrm{AlN})_n/(\mathrm{GaN})_n(0001)$ ($n=3$ and 5) heterostructures. For HM, the absolute DOS value at the Fermi level is also shown in parentheses, in units of states/cell eV.

| | GGA | | | | LDA | | | |
|---|---|---|---|---|---|---|---|---|
| Concentration (ML) | MM ($\mu_B$) | $E^f_{\mathrm{metal}}$ (eV) | $E^f_{\mathrm{N_2}}$ (eV) | $P$ (%) | MM ($\mu_B$) | $E^f_{\mathrm{metal}}$ (eV) | $E^f_{\mathrm{N_2}}$ (eV) | $P$ (%) |
| | | | | $(\mathrm{AlN})_3/(\mathrm{GaN})_3(0001)$ | | | | |
| 1 | 2.16 | 1.76 | 1.24 | 64 | 2.03 | 2.65 | 1.92 | 56 |
| 1/2 | 2.96 | 1.91 | 1.39 | HM (45) | 2.84 | 2.81 | 2.08 | HM (41) |
| 1/4 | 2.97 | 1.98 | 1.46 | HM (57) | 2.81 | 2.92 | 2.19 | HM (43) |
| | | | | $(\mathrm{AlN})_5/(\mathrm{GaN})_5(0001)$ | | | | |
| 1 | 2.17 | 1.75 | 1.23 | 67 | 2.09 | 1.542 | 1.551 | 48 |
| 1/2 | 2.97 | 1.89 | 1.37 | HM (46) | 2.83 | 1.531 | 1.541 | HM (36) |
| 1/4 | 2.96 | 1.97 | 1.45 | HM (49) | 2.81 | 1.535 | 1.546 | HM (37) |

interface, i.e., Ga5 in the 5+5 supercell (or Ga3 in the 3+3 system). Also interestingly, by contrast, in the AlN region, the center site, i.e., well away from the interface, represents a local minimum for all the cases we investigated. Overall, the GGA and LDA give similar results, in particular, the same energy ordering. As for the single-phase systems, the LDA formation energy is larger than that of the GGA. The present results are in agreement with those observed from the all-electron full-potential linearized augmented plane-wave (FLAPW) method.[38] For the favorable sites, the calculated formation energies, magnetic moments, and degree of spin polarization are summarized in Tables V and VI for the $\delta$-layer Cr- and Mn-doped AlN/GaN(0001) systems.

It is important to note that the calculated formation energies are dependent on the concentration. Lower concentrations lead to higher formation energies for both Cr- and Mn-doped systems, showing that even for the $\delta$-layer doped systems, the dopants prefer to form clusters due to the attractive interaction between the dopants. To determine the magnetic interaction, for pair doping, we calculated both the ferromagnetic (FM) and antiferromagnetic (AFM) solutions for different concentrations and found that the ferromagnetic state is favored for all cases. For example, pair doping of Cr (or Mn) atoms at the favorable layer with the largest distances in $(1\times2):(\mathrm{AlN})_5/(\mathrm{GaN})_5$, $(2\times2):(\mathrm{AlN})_5/(\mathrm{GaN})_5$, and $(2\times4):(\mathrm{AlN})_5/(\mathrm{GaN})_5$ gives an energy difference between FM and AFM orderings of 15, 101, and 58 meV/Cr (14, 113, and 64 meV/Mn). The predicted FM states are in agreement with the band coupling model.[72–74] For both (neutral) Cr- and Mn-doped systems, there is the presence of partially filled gap states (two holes per $\mathrm{Cr}^{3+}$ ion and one hole for the $\mathrm{Mn}^{3+}$ ion), allowing virtual hopping for FM

TABLE VI. MMs on the Mn atom, and the formation energies under metal-rich, $E^f_{\mathrm{metal}}$, and N-rich, $E^f_{\mathrm{N_2}}$, growth conditions, and the spin polarizations $P$ for the energetically most favorable Cr-layer doped $(1\times1)$, $(1\times2)$, and $(2\times2):(\mathrm{AlN})_n/(\mathrm{GaN})_n(0001)$ ($n=3$ and 5) heterostructures. For HM, the absolute DOS value at the Fermi level is also shown in parentheses, in units of states/per cell eV.

| | GGA | | | | LDA | | | |
|---|---|---|---|---|---|---|---|---|
| Concentration (ML) | MM ($\mu_B$) | $E^f_{\mathrm{metal}}$ (eV) | $E^f_{\mathrm{N_2}}$ (eV) | $P$ (%) | MM ($\mu_B$) | $E^f_{\mathrm{metal}}$ (eV) | $E^f_{\mathrm{N_2}}$ (eV) | $P$ (%) |
| | | | | $(\mathrm{AlN})_3/(\mathrm{GaN})_3(0001)$ | | | | |
| 1 | 3.56 | 2.54 | 2.02 | 50 | 3.38 | 3.31 | 3.58 | 46 |
| 1/2 | 3.82 | 2.90 | 2.38 | HM (76) | 3.44 | 3.72 | 2.99 | HM (71) |
| 1/4 | 3.80 | 3.05 | 2.53 | HM (97) | 3.59 | 3.92 | 3.19 | HM (110) |
| | | | | $(\mathrm{AlN})_5/(\mathrm{GaN})_5(0001)$ | | | | |
| 1 | 3.71 | 2.52 | 2.00 | 69 | 3.50 | 3.28 | 3.55 | 62 |
| 1/2 | 3.80 | 2.91 | 2.39 | HM (82) | 3.61 | 3.70 | 2.96 | HM (78) |
| 1/4 | 3.82 | 3.03 | 2.51 | HM (91) | 3.62 | 3.91 | 3.18 | HM (85) |

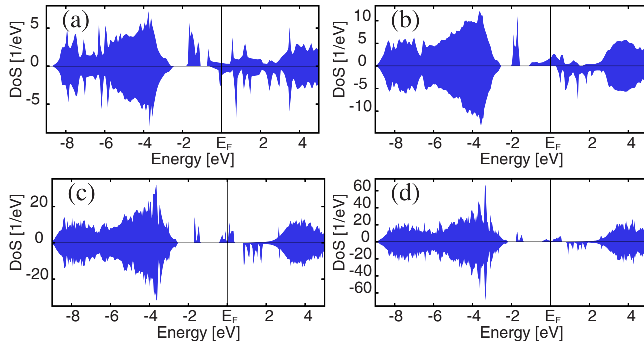

FIG. 5. (Color online) Total density of states for Cr-doped (a) $(1\times1)$, (b) $(1\times2)$, (c) $(2\times2):(AlN)_3/(GaN)_3(0001)$, and (d) $(2\times2):(AlN)_5/(GaN)_5(0001)$ heterostructures, as obtained using the GGA.

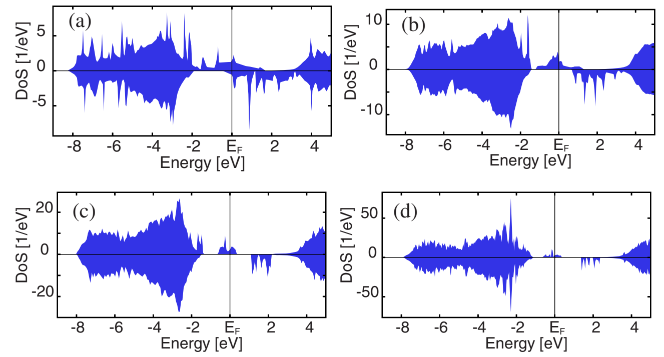

FIG. 6. (Color online) Total density of states for Mn-doped (a) $(1\times1)$, (b) $(1\times2)$, (c) $(2\times2):(AlN)_3/(GaN)_3(0001)$, and (d) $(2\times2):(AlN)_5/(GaN)_5(0001)$ heterostructures, as obtained using the GGA.

arrangement. The FM interaction between $d$ orbitals is further evidenced by the antiparallel moment on the N atoms between the Cr or Mn atoms, namely, about $-0.02\mu_B$ and $-0.06\mu_B$ for the Cr- and Mn-doped systems. We also investigated doping with three Cr (and Mn) atoms with the closest in-plane clustering triangular configuration in the $(4\times4):(AlN)_3/(GaN)_3$ (192-atom cell) and $(2\times2):(AlN)_5/(GaN)_5$ (80-atom cell) systems and found that FM is always preferred over the partially AFM coupling[48] by 23 and 42 meV/Cr for the Cr-doped systems, respectively, and 37 and 51 meV/Mn for Mn-doped heterostructures.

The magnetic moments on Cr and Mn atoms in the $(1\times1)$ (1 ML) structures are found to be much smaller than those in the $(1\times2)$ (1/2 ML) and $(2\times2)$ (1/4 ML) structures, where those for the latter two systems are similar; see Tables V and VI. The lower moments for the $(1\times1)$ heterostructures are due to the strong magnetic interactions between the neighboring supercells. By contrast, the dopants in the $(2\times2)$ structure in 3+3 and 5+5 heterostructures represent the case of a more isolated dopant, resulting in $3\mu_B$/cell and $4\mu_B$/cell with the moment predominantly on the Cr and Mn atoms, respectively, as found in Cr:GaN and Cr:AlN.[34,47] The GGA gives slightly larger atomic magnetic moments than the LDA. Unlike the band gap, which is mainly due to the volume effect as mentioned earlier, we found that even for the same structure and volume, the GGA always gives slightly larger atomic moments than the LDA. However, for the total magnetic moment per $(2\times2)$ supercell, both GGA and LDA give consistent integer values.

The total DOSs for Cr- and Mn-doped $(1\times1)$:3+3, $(1\times2)$:3+3, $(2\times2)$:3+3, and $(2\times2)$:5+5 heterostructures are shown in Figs. 5 and 6, respectively, where the Cr and Mn 3$d$ bands are located in the band gap of the host semiconductors. Importantly, our results clearly demonstrate the dependence of the electronic character (and hence conductivity) on the doping concentration: While the $(1\times2)$ and $(2\times2):(AlN)_n/(GaN)_n(0001)$ ($n$=3 and 5) (0001) heterostructures exhibit the appealing HM, the Cr- and Mn-doped $(1\times1):(AlN)_n/(GaN)_n(0001)$ ($n$=3 and 5) are in fact metallic. Recalling the clustering tendency mentioned earlier, such behavior will lead to local high concentrations such as those representative of the $(1\times1)$ structures, which may destroy the HM and degrade injection efficiency and performance.

At the high concentration of 1 ML $\delta$ doping of Cr and Mn, the heterostructures are predicted to show typical metallic character, rather than half-metallic states, due to the strong interaction between transition-metal atoms. However, with lower concentrations, 1/2 and 1/4 ML, the appealing HM is observed. Interestingly, such HM is found to be rather robust for even lower concentrations. In particular, the HM is also retained for the $(4\times4):(AlN)_3/(GaN)_3(0001)$ (192-atom supercell) heterostructure, corresponding to a 1/16 ML concentration. Notably, for Cr-doped bulk GaN (or AlN), decreasing doping concentration (using a larger supercell) leads to the system change from HM to semiconducting.[48] This is because in these systems the Fermi level is typically located in the valley (with small DOS) between the occupied 1/3 $t_2$ ($d_{xy}$) and the unoccupied 2/3 $t_2$ ($d_{xz},d_{yz}$), with these two unoccupied orbitals being almost degenerate, as expected from symmetry consideration. The presence of the valley, or the splitting within the $t_2$, is due to the Jahn-Teller effect. As the doping concentration decreases, the interaction between the dopants in the neighboring cells is weakened, giving rise to more discrete levels. However, for the Cr-doped AlN/GaN interface systems, lower symmetry leads to a broadening of the DOS around $E_F$ (higher DOS at the valley), and consequently a more robust HM as compared to the Cr-doped bulk GaN (or AlN). Based on this simple argument, one can understand that for (neutral) Mn-doped III nitrides and heterostructures, the HM is more robust against lower concentrations than Cr-doped systems because now the Fermi level $E_F$ is located between the $d_{xz}$ and $d_{yz}$ orbitals. This can be seen from the DOS (Figs. 5 and 6) and the calculated spin polarization in Tables V and VI, where the absolute DOSs for the HM states are considerably larger for the Mn-doped heterostructures compared to the Cr-doped ones. For a given system, we also compared the DOSs for the various alternative dopant sites and found that the result is almost unchanged, even irrespective of whether the doped site is Al or Ga.

To have a closer look at the electronic structure change upon doping, we show the total and atom-resolved band structures in different layers for both systems under different concentrations, as shown in Figs. 7 and 8. In particular, layer-resolved band structures help one to understand the

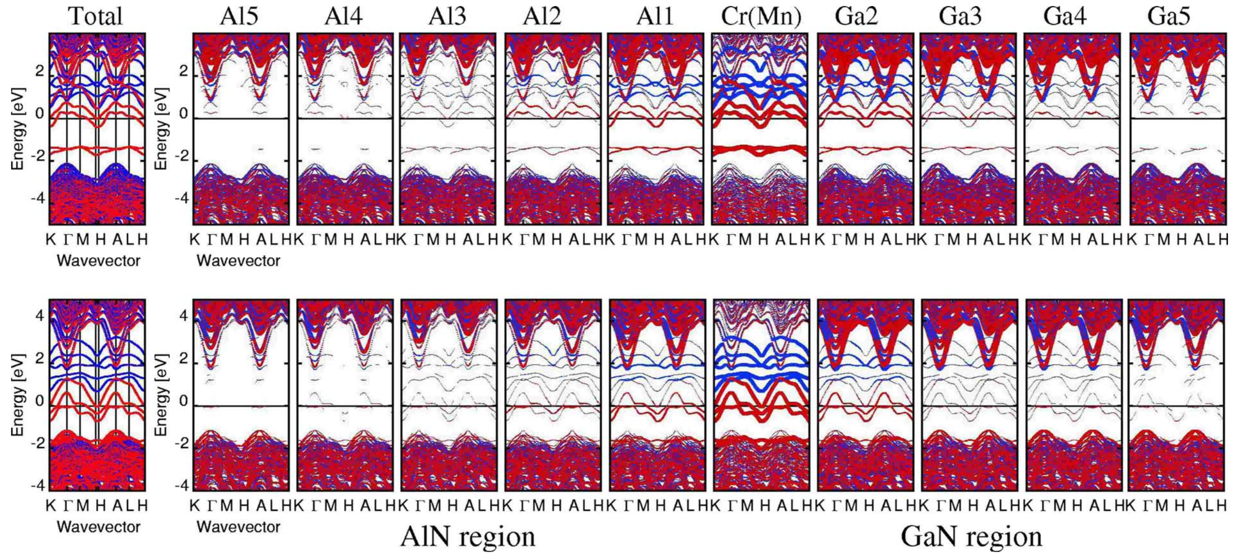


FIG. 7. (Color online) Total and atom-resolved band structures for Cr- (upper panel) and Mn-doped (lower panel) $(AlN)_5/(GaN)_5(0001)$ heterostructures at the concentration of 1/2 ML, as obtained using the GGA. Red denotes majority bands, and blue denotes minority bands.

mechanism of DMS-based spin injection. Here we illustrate this process by taking the Cr- and Mn-doped 5+5 heterostructures at 1/2 ML concentration as examples. Similar arguments apply to 1 and 1/4 ML concentrations, for which we only show the band structures from Cr and Mn atoms in Fig. 8.

The total band structures clearly show that the doped Cr and Mn atoms introduce $3d$ orbitals typically lying in the band gap of the host heterostructures. For both the majority (in red) and minority (in blue) bands, the lower lying are the two $e$ orbitals and higher are the three $t_2$ orbitals. For high concentration, i.e., 1 ML, both Cr- and Mn-doped systems show that these $d$ orbitals are dispersed and result in metallic states. At 1/2 and 1/4 ML, both systems are half metallic, with the 1/4 ML orbital being much more localized (flat).

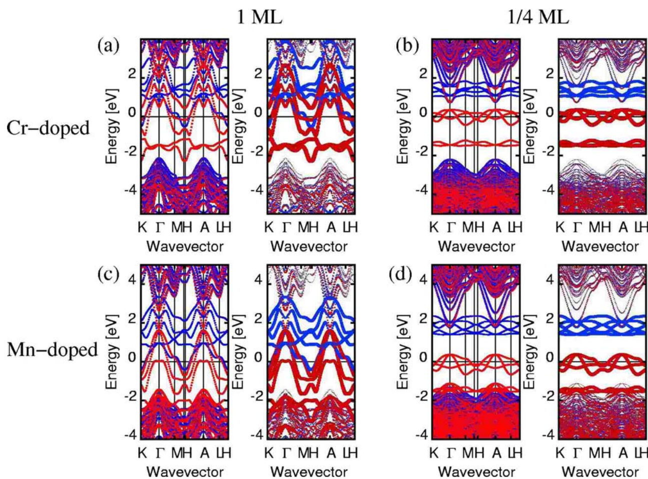


FIG. 8. (Color online) Total and dopant band structures for Cr- (upper panel) and Mn-doped (lower panel) $(AlN)_5/(GaN)_5(0001)$ heterostructures at the concentrations of 1 and 1/4 ML, as obtained using the GGA. For each system, the left (right) panel is the total (Cr- or Mn-resolved) band structure.

While for Cr-doped systems, the majority $e$ orbitals are lying within the band gap, for Mn-doped systems, these low-lying $e$ orbitals have strong a coupling with the valence-band maximum of the host heterostructure. The magnetic dopants interact with the host heterostructures via hybridization with the surrounding atoms in a range up to several layers, as can be seen from the layer-resolved band structures. The dopants $3d$ orbitals couple strongly with nearby N $2p$ and Al (or Ga) $3s$ and $3p$ states. Projected band-structure analysis reveals that N $2p$ states mainly couple with $e$ orbitals and the interaction with $t_2$ orbitals are negligible. Considering that it is the $t_2$ orbital electrons that are responsible for the spin injection, for simplicity, we omit the N-atom contribution in the layer-resolved band structures in Fig. 7. Since this hybridization occurs in both sides of the interfaces, and the $t_2$ orbital serves as the transport channel, spin injection can occur via diffusion from a doped GaN region into AlN, free of the conductivity mismatch problem known for traditional metal/semiconductor interfaces. This, in turn, suggests that this mechanism requires the dopant layer to be close to the interface. One can also see that in the AlN region close to the interfaces (Al5 and Al1), the conduction-band minima (CBM) are lowered due to interaction between the Al $3s$ and Ga $3s$ orbitals mediated by N $2p$ states. Far away from the interfaces, the AlN region (Al3) acts like the bulk semiconductor and serves as the tunnel barrier for the injected spin-polarized electrons. Because DFT underestimates the band gap, in real devices, the CBM could be much higher, which would tend to favor the tunneling transport of spin-polarized electrons over a longer distance. In this light, we predict that the 1/4 ML concentration in which the $d$ orbitals are more localized, is easier for tunneling than 1/2 and 1 ML.

Importantly, after doping Cr or Mn, the built-in electric field remains largely unchanged. The average N-atom $1s$ core-level binding energies $E_b^{\mathrm{CL}}$ within each layer for the energetically most favorable 1/2 ML Cr- and Mn-doped AlN/GaN(0001) heterostructures are shown in Fig. 3. Only around the interface for the Cr-doped system is there a siz-

able increase in the electric field. Significantly, for the energetically most favorable $\delta$-layer doped heterostructures where the dopants are located at the negative slope of the core-level binding energies curve, as indicated by the arrows in Fig. 3, there is a spontaneous driving force to push the spin-polarized electrons injecting from the GaN region into the AlN region. For other dopant sites in the GaN region, the electric field will in fact tend to oppose the injection to the AlN region through the type-A interface. This further shows that for optimal devices, it is preferable that the dopants are located in the GaN region, close to the type-A interface, i.e., at the Ga1 layer. Furthermore, once the spin-polarized electrons have crossed the interface, there is still an electric force in the AlN region, facilitating the spin transport and minimizing the spin dephasing.

### 2. Charged states

So far we have only considered neutral states. However, for transition-metal-doped III-V systems, for example, Mn-doped GaN, both experiments[75–77] and calculations[34] show that the Mn at the substitutional cation site can also exist as negatively charged $Mn^{2+}$ in addition to the neutral state $Mn^{3+}$ (analogous to $Ga^{3+}$ in bulk GaN). As found in Mn-doped bulk GaN,[34] charged states will typically exhibit distinctive behavior in magnetic coupling and electronic structures as compared with the neutral states. In this study, we investigate both Cr- and Mn-doped $(AlN)_5/(GaN)_5(0001)$ heterostructures with $(1\times1)$, $(1\times2)$, and $(2\times2)$ supercells using the GGA. We aim to determine the stable valence states, the magnetic coupling, and the DOS (consequently the degree of spin polarization).

The calculated formation energies under N-rich growth conditions are shown in Fig. 9. For both Cr- and Mn-doped systems, our results predict that the dopants can be stabilized in various valence states depending on the Fermi level, i.e., $n$ type or $p$ type of the host semiconductor. That is, both the Cr and Mn ions can in principle be stabilized as neutral states ($Cr^{3+}$ and $Mn^{3+}$), as well as positively charged states ($Cr^{4+}$ and $Mn^{4+}$) and negatively charged states ($Cr^{2+}$ and $Mn^{2+}$). Interestingly, it is found that higher dopant concentrations lead to lower formation energies for both neutral and charged states due to the attractive interactions between dopants. The energy differences between various concentrations are less significant for charged states due to the repulsive Coulomb forces between the identical types of charged ions. Importantly, as the concentration increases from 1/4 to 1 ML, the transition levels $(+1/0)$ and $(0/1-)$ are shifted to lower and higher energies, respectively, showing that higher concentrations tend to favor the neutral states. More specifically, for the Cr-doped system, besides the neutral state $Cr^{3+}\,3d^3$ $(e^2t_2^1)$, for all concentrations considered, the positively charged state $Cr^{4+}\,3d^2$ $(e^2t_2^0)$ is predicted to be stable under $p$-type conditions. For lower concentrations (1/2 and 1/4 ML), the negatively charged $Cr^{2+}\,3d^4$ $(e^2t_2^2)$ state is also stable, while for the metallic 1 ML case, such a state is not stable.

For the Mn-doped system, we find that positively charged $Mn^{4+}\,3d^3$ $(e^2t_2^1)$, neutral $Mn^{3+}\,3d^4$ $(e^2t_2^2)$, and negatively charged $Mn^{2+}\,3d^5$ $(e^2t_2^3)$ are all stable, depending on the position of the Fermi level. Note that for Cr-doped GaN,[78,79] experiments so far report detection of only neutral ions, while for Mn-doped GaN, both $Mn^{3+}\,3d^4$ and $Mn^{2+}\,3d^5$ (dominant) are observed.[75–77] Presumably, this may be due to the well-known fact that as-grown GaN is usually $n$ type (with a surplus of electrons), and $p$-type conductivity is more difficult to obtain.[80] In addition, for the $Cr^{2+}$ state, the positions of the transition level $(0/-1)$ are quite high, namely, 2.7 and 2.9 eV for 1/4 and 1/2 ML, respectively. In fact, if we consider the range of $E_F$ from 0 to the calculated band gap 2.91 eV, such transition levels are edged out or very close to the conduction-band minimum.

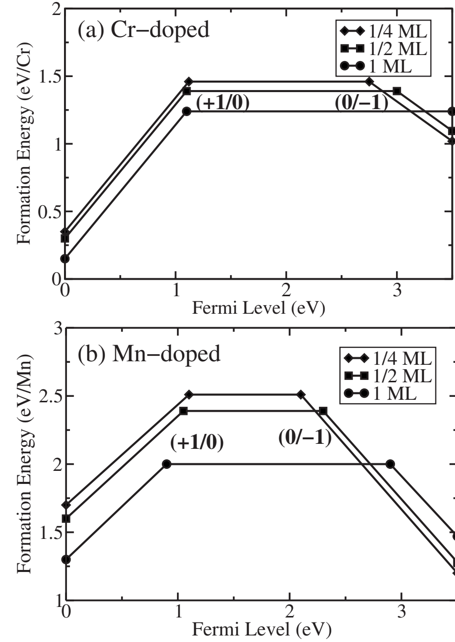


FIG. 9. Formation energies (under N-rich conditions) for neutral and charged states of (a) Cr-doped and (b) Mn-doped $(AlN)_5/(GaN)_5(0001)$ heterostructures with different doping concentrations, as obtained using the GGA.

For the stable valence states, the calculated magnetic moments, the energy difference between FM and AFM states [calculated in $(1\times2)$, $(2\times2)$, and $(2\times4)$ supercells], and the degree of SP, are collected in Table VII. We first confirm that for the neutral states, both Cr- and Mn-doped systems at various concentrations are all FM—an essential requirement for spin injection electrodes. Importantly, we point out that the effects of the charged states on the magnetic coupling for Cr-doped and Mn-doped heterostructures are strikingly different: the positively charged states make the magnetic interaction between two Cr ions ($Cr^{4+}\,3d^2$) to be AFM and between two Mn ions ($Mn^{4+}\,3d^3$) to be FM. By contrast, the negatively charged states lead the coupling between two Cr ions ($Cr^{2+}\,3d^4$) to be FM and between two Mn ions ($Mn^{2+}\,3d^5$) to be AFM. Such an interesting behavior for the magnetic coupling of the neutral and charged ions is in accordance with the band coupling model,[72–74] which predicts FM with the presence of partially filled gap states.

Substitutional doped Cr and Mn ions at cation sites are bonded tetrahedrally to the four neighboring nitrogen atoms. The tetrahedral crystal field of the surrounding N ligands

TABLE VII. MMs on Cr and Mn sites, the energy difference between FM and AFM states, $\Delta E_{\text{FM-AFM}}$, and the degree of spin polarization $P$ for the energetically most favorable $\delta$-layer Cr- and Mn-doped $(1\times1)$, $(1\times2)$, and $(2\times2)$:$(\text{AlN})_5/(\text{GaN})_5(0001)$ heterostructures, as obtained using the GGA. For HM, the absolute DOS value at the Fermi level is also shown in parentheses, in units of states/per cell eV. Semiconducting behavior corresponds to $P=0$.

| Concentration (ML) | Valence states | MM ($\mu_B$/Cr) | $\Delta E_{\text{FM-AFM}}$ (meV/Cr) | $P$ (%) |
|---|---|---|---|---|
| Cr-doped $(\text{AlN})_5/(\text{GaN})_5$ heterostructure | | | | |
| 1 | $+1(d^2)$ | 2.53 | 178 | 7 |
| | $0(d^3)$ | 2.17 | −15 | 67 |
| | $-1(d^4)$ | 2.89 | −105 | 31 |
| 1/2 | $+1(d^2)$ | 2.28 | 132 | 4 |
| | $0(d^3)$ | 2.97 | −101 | HM (46) |
| | $-1(d^4)$ | 3.76 | −72 | HM (38) |
| 1/4 | $+1(d^2)$ | 2.04 | 93 | 0 |
| | $0(d^3)$ | 2.96 | −58 | HM (49) |
| | $-1(d^4)$ | 3.77 | −46 | 0 |
| Mn-doped $(\text{AlN})_5/(\text{GaN})_5$ heterostructure | | | | |
| 1 | $+1(d^3)$ | 2.06 | −88 | 10 |
| | $0(d^4)$ | 3.71 | −14 | 69 |
| | $-1(d^5)$ | 3.39 | 189 | 11 |
| 1/2 | $+1(d^3)$ | 3.12 | −67 | 41 |
| | $0(d^4)$ | 3.80 | −113 | HM (82) |
| | $-1(d^5)$ | 4.48 | 163 | 53 |
| 1/4 | $+1(d^3)$ | 2.93 | −46 | HM (11) |
| | $0(d^4)$ | 3.82 | −64 | HM (91) |
| | $-1(d^5)$ | 4.54 | 132 | 0 |

splits the fivefold-degenerate $3d$ states of the dopant ions into two low-lying $e$ ($d_{z^2}$ and $d_{x^2-y^2}$) and three high-lying $t_2$ ($d_{xy}$, $d_{xz}$, and $d_{yz}$) subsets. For isolated neutral ions in GaN, the ground states are high spin states, corresponding to $3\mu_B$/Cr and $4\mu_B$/Mn.[81] The structural distortion at the interface does not change the band orders, as evidenced from the magnetic moments. So that for Cr ions, each neutral $\text{Cr}^{3+}$ $3d^3$ (and negatively charged $\text{Cr}^{2+}$ $3d^4$) ion has two holes (and one hole) in the spin-up channel, consequently leading to a FM coupling. Similarly for Mn ions, each neutral $\text{Mn}^{3+}$ $3d^4$ (and positively charged $\text{Mn}^{4+}$ $3d^3$) ion has one hole (and two holes) in the spin-up channel, and also lead to a FM coupling. By contrast, the magnetic interactions between two $\text{Cr}^{4+}$ $3d^2$ ions and between two $\text{Mn}^{2+}$ $3d^5$ ions in the doped $x$-$y$ plane are AFM. This is because now $\text{Cr}^{4+}$ and $\text{Mn}^{2+}$ ions have $e^2t_2^0$ and $e^2t_2^5$ configurations and, thus, have no partially filled gap states; consequently, virtual hopping is allowed in the AFM arrangement.

Since charged states will change the position of the Fermi level, as expected, it will have a profound effect on the electronic structure and consequently on the conductivity. In view of the application as electrodes for spin injection, here we focus on the stable charged state ions with FM ground

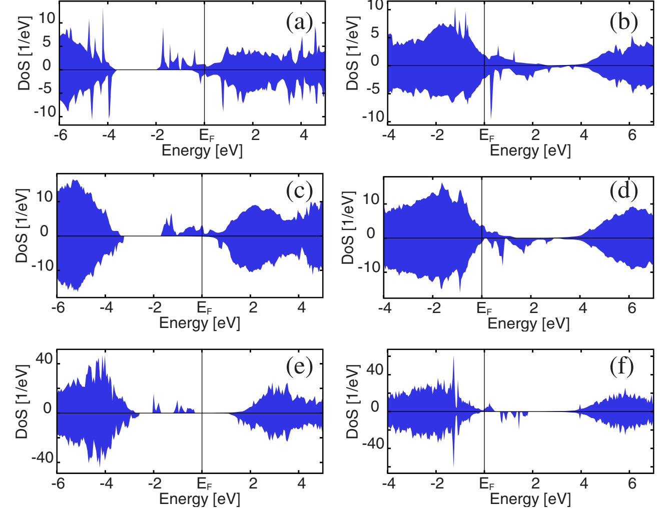


FIG. 10. (Color online) Total density of states for ferromagnetic charged states: left column is for $\text{Cr}^{2+}$ and right column is for $\text{Mn}^{4+}$ for different concentrations: [(a) and (b)] 1 ML, [(c) and (d)] 1/2 ML, and [(e) and (f)] 1/4 ML, as obtained using the GGA.

states. The DOSs for the FM states at different concentrations for both systems are shown in Fig. 10. In particular, for the FM interacting $\text{Cr}^{2+}$ ions, the DOSs show the distinct metallic, half-metallic, and semiconducting behaviors for 1, 1/2, and 1/4 ML, respectively. For the half metallic 1/2 ML, the DOS value of the spin-up state at the Fermi level is smaller (38 states/eV per supercell) than the corresponding neutral state (46 states/eV per supercell), which is expected to have lower spin injection efficiency. For the metallic 1 ML concentrations, the negatively charged state also leads to a smaller value of spin polarization (31%) as compared with the neutral one (67%). For the FM interacting $\text{Mn}^{4+}$ ions, 1/2 ML concentration is predicted to be metallic state, rather than half metallic for the neutral state. For the metallic state 1 ML concentration, the SP values are significantly smaller than the one for the neutral state. For the half-metallic 1/4 ML concentration, the DOS value of the spin-up state at the Fermi level is also smaller than the corresponding neutral state, dropping from 91 to 11 states/eV per supercell.

Thus, in view of the two essential requirements for potential electrodes—being FM and with high SP—we conclude that for both Cr- and Mn-doped AlN/GaN heterostructures, charged states will not help in achieving the appealing HM and will be destructive for efficient spin injection, and thus, potential optimal materials should be designed to contain these dopants in the neutral state.

## IV. SUMMARY AND CONCLUSION

Highly spin-polarized materials, such as half-metallic ferromagnets, would provide effective spin injection into nonmagnetic semiconductors and are important for nonvolatile memory applications. Unlike using the traditional metal electrode as a spin aligner, in which the discontinuities in atomic environment and consequently in band alignment are two intrinsic factors affecting the spin polarization and hence

spin injection efficiency, the interface problem using DMSs is expected to be less serious due to the coherent chemical and conductive properties between the DMS and semiconductor. However, to fulfill the potential of DMS for spin injection and optimal performance, one needs to consider various different aspects and challenges, mainly arising from the DMS itself—such as spatial dopant distribution, dopant concentration, growth conditions, and possible different valence states.

To address these fundamental issues and to shed light on some possible routes in aiming for an improved room-temperature spin injection using DMS, we have performed first-principles calculations for pure and $\delta$-layer Cr- and Mn-doped AlN/GaN(0001) heterostructures using both the LDA and the GGA for the exchange-correlation functional. The semiconducting property of AlN and GaN is retained in the pure AlN/GaN(0001) heterostructures, where the electronic band gap decreases monotonically with the thickness of the superlattice due to the strong built-in electric field. For both Cr- and Mn-doped systems, the doped atoms prefer to segregate into the GaN region and reside close to the interface under both nitrogen-rich and metal-rich growth conditions. Importantly, we examined the correlation between conductivity and the dopant concentration and the effect of the superlattice size, both along and perpendicular to the epitaxial growth directions. It is found that the half-metallic character of the interface depends sensitively on the dopant concentration and valence charged state. For both Cr- and Mn-doped neutral systems, a 1 ML dopant concentration will lead to a metallic state, while 1/2 and 1/4 ML and even lower concentrations will exhibit half metallicity. The doped Cr and Mn atoms introduce $3d$ states in the band gap of the host semiconductor heterostructure. The spin injection channels are constructed via the hybridization between dopant $3d$ and surrounding host atoms, up to a few monolayers around the interface, where the spin-polarized $t_2$ electrons are injected into AlN without the conductivity mismatch problem. In general, charged states will not help for achieving the appealing HM and will be destructive for efficient spin injection. Moreover, both pure and neutral doped AlN/GaN(0001) heterostructures possess large spontaneous and piezoelectric polarization fields that could actually be utilized for enhanced injection efficiency and possibly other device applications. For the energetically favorable doping configuration, the built-in electric field assists spin injection through the interface, and also spin transport in AlN region.

## ACKNOWLEDGMENTS

We acknowledge the computing resources provided by the Australian Partnership for Advanced Computing (APAC) National Facility and by the Australian Centre for Advanced Computing and Communications (AC3), and support from the Australian Research Council and from the NSF (U.S.) (through its MRSEC program at the Northwestern Materials Research Center).


[1] P. R. Hammar, B. R. Bennett, M. J. Yang, and M. Johnson, Phys. Rev. Lett. **83**, 203 (1999); F. G. Monzon and M. L. Roukes, J. Magn. Magn. Mater. **198–199**, 632 (1999); D. Hagele, M. Oestreich, W. W. Ruhle, N. Nestle, and K. Eberl, Appl. Phys. Lett. **73**, 1580 (1998).

[2] H. Ohno, Science **281**, 951 (1998); S. A. Wolf, D. D. Awschalom, R. A. Buhrman, J. M. Daughton, S. von Molnar, M. L. Roukes, A. Y. Chtchelkanova, and D. M. Treger, *ibid.* **294**, 1488 (2001).

[3] I. Zutic, J. Fabian, and S. D. Sarma, Rev. Mod. Phys. **76**, 323 (2004).

[4] D. D. Awschalom and M. E. Flatte, Nat. Phys. **3**, 153 (2007).

[5] F. Meier and B. P. Zakharchenya, *Optical Orientation* (North Holland, Amsterdam, Netherlands, 1984), Vol. 8.

[6] G. Schmidt, D. Ferrand, L. W. Molenkamp, A. T. Filip, and B. J. van Wees, Phys. Rev. B **62**, R4790 (2000).

[7] E. I. Rashba, Phys. Rev. B **62**, R16267 (2000).

[8] A. T. Filip, B. H. Hoving, F. J. Jedema, B. J. van Wees, B. Dutta, and S. Borghs, Phys. Rev. B **62**, 9996 (2000).

[9] A. Fert and H. Jaffres, Phys. Rev. B **64**, 184420 (2001).

[10] M. R. Hofmann and M. Oestreich, *Ferromagnet/Semiconductor Heterostructures and Spin Injection*, Springer Tracts in Modern Physics Vol. 227 (Springer, Berlin, 2007), pp. 335–360.

[11] B. J. van Wees, Nat. Phys. **3**, 147 (2007).

[12] R. A. de Groot, F. M. Mueller, P. G. van Engen, and K. H. J. Buschow, Phys. Rev. Lett. **50**, 2024 (1983).

[13] Ph. Mavropoulos and I. Galanakis, J. Phys.: Condens. Matter **19**, 315221 (2007).

[14] S. Fujii, S. Sugimura, S. Ishida, and S. Asano, J. Phys.: Condens. Matter **2**, 8583 (1990).

[15] S. Picozzi, A. Continenza, and A. J. Freeman, Phys. Rev. B **66**, 094421 (2002).

[16] A. Hirohata, M. Kikuchi, N. Tezuka, K. Inomata, J. S. Claydon, Y. B. Xu, and G. van der Laan, Curr. Opin. Solid State Mater. Sci. **10**, 93 (2006).

[17] D. Orgassa, H. Fujiwara, T. C. Schulthess, and W. H. Butler, Phys. Rev. B **60**, 13237 (1999).

[18] M. P. Raphael, B. Ravel, Q. Huang, M. A. Willard, S. F. Cheng, B. N. Das, R. M. Stroud, K. M. Bussmann, J. H. Claassen, and V. G. Harris, Phys. Rev. B **66**, 104429 (2002); B. Ravel, J. O. Cross, M. P. Raphael, V. G. Harris, R. Ramesh, and V. Saraf, Appl. Phys. Lett. **81**, 2812 (2002).

[19] S. Picozzi and A. J. Freeman, J. Phys.: Condens. Matter **19**, 315215 (2007).

[20] N. Ghaderi, S. J. Hashemifar, H. Akbarzadeh, and M. Peressi, J. Appl. Phys. **102**, 074306 (2007).

[21] C. Gould, G. Schmidt, G. Richter, R. Fiederling, P. Grabs, and L. W. Molenkamp, Appl. Surf. Sci. **190**, 395 (2002).

[22] J. C. Egues, Phys. Rev. Lett. **80**, 4578 (1998).

[23] R. Fiederling, M. Keim, G. Reuscher, W. Ossau, G. Schmidt, A. Waag, and L. W. Molenkamp, Nature (London) **402**, 787 (1999).

[24] M. Oestreich, J. Hubner, D. Hagele, P. J. Klar, W. Heimbrodt, W. W. Ruhle, D. E. Ashenford, and B. Lunn, Appl. Phys. Lett. **74**,

1251 (1999).

[25] Y. Ohno, D. K. Young, B. Beschoten, F. Matsukura, H. Ohno, and D. D. Awschalom, Nature (London) **402**, 790 (1999).

[26] T. Dietl, H. Ohno, F. Matsukura, J. Cibert, and D. Ferrand, Science **287**, 1019 (2000).

[27] M. Hashimoto, Y. K. Zhou, M. Kanamura, and H. Asahi, Solid State Commun. **122**, 37 (2002).

[28] S. E. Park, H. J. Lee, Y. C. Cho, S. Y. Jeong, C. R. Cho, and S. Cho, Appl. Phys. Lett. **80**, 4187 (2002).

[29] H. X. Liu, S. Y. Wu, R. K. Singh, L. Gu, D. J. Smith, N. Newman, N. R. Dilley, L. Montes, and M. B. Simmonds, Appl. Phys. Lett. **85**, 4076 (2004).

[30] R. K. Singh, S. Y. Wu, H. X. Liu, L. Gu, D. J. Smith, and N. Newman, Appl. Phys. Lett. **86**, 012504 (2005).

[31] T. Sasaki, S. Sonoda, Y. Yamamoto, K. Suga, S. Shimizu, K. Kindo, and H. Hori, J. Appl. Phys. **91**, 7911 (2002).

[32] N. Theodoropoulou, A. F. Hebard, M. E. Overberg, C. R. Abernathy, S. J. Pearton, S. N. G. Chu, and R. G. Wilson, Appl. Phys. Lett. **78**, 3475 (2001).

[33] K. Sato, W. Schweika, P. H. Dederichs, and H. Katayama-Yoshida, Phys. Rev. B **70**, 201202(R) (2004).

[34] X. Y. Cui, B. Delley, A. J. Freeman, and C. Stampfl, Phys. Rev. B **76**, 045201 (2007).

[35] B. Beschoten, E. Johnston-Halperin, D. K. Young, M. Poggio, J. E. Grimaldi, S. Keller, S. P. DenBaars, U. K. Mishra, E. L. Hu, and D. D. Awschalom, Phys. Rev. B **63**, 121202(R) (2001).

[36] S. Krishnamurthy, M. van Schilfgaarde, and N. Newman, Appl. Phys. Lett. **83**, 1761 (2003).

[37] H. Katayama-Yoshida and K. Sato, Physica B **327**, 337 (2003); L. Kronik, M. Jain and J. R. Chelikowsky, Phys. Rev. B **66**, 041203(R) (2002).

[38] J. E. Medvedeva, A. J. Freeman, X. Y. Cui, C. Stampfl, and N. Newman, Phys. Rev. Lett. **94**, 146602 (2005).

[39] A. Debernardi, Superlattices Microstruct. **40**, 530 (2006).

[40] M.-S. Kim, Y.-K. Zhou, M. Funakoshi, S. Emura, S. Hasegawa, and Hajime Asahi, Appl. Phys. Lett. **89**, 232511 (2006).

[41] M.-H. Ham, S. Yoon, Y. Park, L. Bian, M. Ramsteiner, and Jae-Min Myoung, J. Phys.: Condens. Matter **18**, 7703 (2006).

[42] T. Takeuchi, Y. Harada, T. Tokushima, M. Taguchi, Y. Takata, A. Chainani, J. J. Kim, H. Makino, T. Yao, T. Yamamoto, T. Tsukamoto, S. Shin, and K. Kobayashi, Phys. Rev. B **70**, 245323 (2004).

[43] R. M. Frazier, G. T. Thaler, J. Y. Leifer, J. K. Hite, B. P. Gila, C. R. Abernathy, and S. J. Pearton, Appl. Phys. Lett. **86**, 052101 (2005).

[44] S. Dhar, O. Brandt, A. Trampert, K. J. Friedland, Y. J. Sun, and K. H. Ploog, Phys. Rev. B **67**, 165205 (2003).

[45] V. A. Guzenko, N. Thillosen, A. Dahmen, R. Calarco, Th. Schapers, L. Houben, M. Luysberg, B. Schineller, M. Heuken, and A. Kaluza, J. Appl. Phys. **96**, 5663 (2004).

[46] L. Gu, S. Y. Wu, H. X. Liu, R. K. Singh, N. Newman, and D. J. Smith, J. Magn. Magn. Mater. **290–291**, 1395 (2005).

[47] X. Y. Cui, J. E. Medvedeva, B. Delley, A. J. Freeman, N. Newman, and C. Stampfl, Phys. Rev. Lett. **95**, 256404 (2005).

[48] X. Y. Cui, J. E. Medvedeva, B. Delley, A. J. Freeman, and C. Stampfl, Phys. Rev. B **75**, 155205 (2007).

[49] E. F. Schubert, J. Vac. Sci. Technol. A **8**, 2980 (1990).

[50] K. Sato, T. Fukushima, and H. Katayama-Yoshida, J. Phys.: Condens. Matter **19**, 365212 (2007).

[51] H. Katayama-Yoshida, K. Sato, T. Fukushima, M. Toyoda, H. Kizaki, V. A. Dinh, and P. H. Dederichs, J. Magn. Magn. Mater. **310**, 2070 (2007).

[52] V. I. Litvinov, Phys. Rev. B **76**, 245305 (2007).

[53] F. Bernardini, V. Fiorentini, and D. Vanderbilt, Phys. Rev. B **56**, R10024 (1997).

[54] V. Fiorentini, F. Bernardini, F. Della Sala, A. Di Carlo, and P. Lugli, Phys. Rev. B **60**, 8849 (1999).

[55] C. Buchheim, R. Goldhahn, A. T. Winzer, G. Gobsch, U. Rossow, D. Fuhrmann, A. Hangleiter, F. Furtmayr, and M. Eickhoff, Appl. Phys. Lett. **90**, 241906 (2007).

[56] J. P. Perdew and Y. Wang, Phys. Rev. B **45**, 13244 (1992).

[57] J. P. Perdew, K. Burke, and M. Ernzerhof, Phys. Rev. Lett. **77**, 3865 (1996).

[58] B. Delley, J. Chem. Phys. **113**, 7756 (2000); J. Chem. Phys. **92**, 508 (1990).

[59] B. Delley, Phys. Rev. B **66**, 155125 (2002).

[60] X. Y. Cui, D. Fernandez-Hevia, B. Delley, A. J. Freeman, and C. Stampfl, J. Appl. Phys. **101**, 103917 (2007).

[61] C. G. Van de Walle, J. Appl. Phys. **95**, 3851 (2004).

[62] A. Zoroddu, F. Bernardini, P. Ruggerone, and V. Fiorentini, Phys. Rev. B **64**, 045208 (2001).

[63] C. Stampfl and C. G. Van de Walle, Phys. Rev. B **59**, 5521 (1999).

[64] K. Kim, W. R. L. Lambrecht, and B. Segall, Phys. Rev. B **53**, 16310 (1996), and references therein.

[65] R. D. Shannon, Acta Crystallogr., Sect. A: Cryst. Phys., Diffr., Theor. Gen. Crystallogr. **32**, 751 (1976).

[66] S. H. Ke, K. M. Zhang, and X. D. Xie, J. Appl. Phys. **80**, 2918 (1996).

[67] We have confirmed that this result is reproducible with all-electron calculations for up to 10+10 superlattices using both $DMol^3$ and FLAPW codes. For the latter code, see E. Wimmer, H. Krakauer, M. Weinert, and A. J. Freeman, Phys. Rev. B **24**, 864 (1981).

[68] S. Picozzi, A. Continenza, and A. J. Freeman, Phys. Rev. B **55**, 13080 (1997).

[69] J. A. Majewski, S. Hackenbuchner, G. Zandler, and P. Vogl, Comput. Mater. Sci. **30**, 81 (2004).

[70] Although it is well known that the absolute Mulliken values are not reliable, it is expected they can predict reliable trends. We also carried out Hirshfeld population analysis and confirmed this trend. All-electron calculations confirm the same picture of charge accumulation at the interfaces, but the Mulliken charge difference values are smaller.

[71] F. Capasso, A. Y. Cho, K. Mohammed, and P. W. Foy, Appl. Phys. Lett. **46**, 664 (1985).

[72] J. Kanamori and K. Terakura, J. Phys. Soc. Jpn. **70**, 1433 (2001).

[73] G. M. Dalpian, S.-H. Wei, X. G. Gong, A. J. R. da Silva, and A. Fazzio, Solid State Commun. **138**, 353 (2006).

[74] B. Belhadji, L. Bergqvist, R. Zeller, P. H. Dederichs, K. Sato, and H. Katayama-Yoshida, J. Phys.: Condens. Matter **19**, 436227 (2007).

[75] T. Graf, M. Gjukic, M. Hermann, M. S. Brandt, M. Stutzmann, and O. Ambacher, Phys. Rev. B **67**, 165215 (2003).

[76] S. Sonoda, I. Tanaka, H. Ikeno, T. Yamamoto, F. Oba, T. Araki, Y. Yamamoto, K. Suga, Y. Nanishi, Y. Akasaka, K. Kindo, and H. Hori, J. Phys.: Condens. Matter **18**, 4615 (2006).

[77] D. J. Keavney, S. H. Cheung, S. T. King, M. Weinert, and L. Li, Phys. Rev. Lett. **95**, 257201 (2005).

[78] J. J. Kim, H. Makino, M. Sakurai, D. C. Oh, T. Hanada, M. W.

Cho, T. Yao, S. Emura, and K. Kobayashi, J. Vac. Sci. Technol. B **23**, 1308 (2005).
[79] S. Subashchandran, S. Kimura, M. S. Kim, S. Kobayashi, Y. K. Zhou, S. Hasegawa, and H. Asahi, Jpn. J. Appl. Phys., Part 2 **45**, 3522 (2006).
[80] H. Amano, M. Kito, K. Hiramutsu, and I. Akasaki, Jpn. J. Appl. Phys., Part 2 **28**, L2112 (1989).
[81] X. Y. Cui, B. Delley, A. J. Freeman, and C. Stampfl, Phys. Rev. Lett. **97**, 016402 (2006).